Journal for ImmunoTherapy of Cancer

Phase I trial of CJRB-101 plus pembrolizumab in patients with metastatic non-small cell lung cancer, head and neck squamous cell carcinoma and melanoma

Jii Bum Lee,[1] Sujeong Baek,[2] Dong Kwon Kim ,[3] Bo-Eun Kwon,[4] Jin Seok Ahn,[5] Misako Nagasaka,[6] Diwakar Davar ,[7] Hyunkyung Park ,[4] Hyunjeong Kim,[4] Jieun Im,[4] Junwon Yang ,[4] Eunchong Yang,[4] Ga-Hyun Shin,[4] Soeun Choi,[4] Ji-Eun Kwon,[4] Jae-Min Kim,[4] So-Yeong Kang,[4] Youngtaek Kim,[3] So Young Park,[2] Jae Hwan Kim,[2,8] Hyun-Seok Oh,[4] Mauricio Chalita,[4] Arim Min,[4] Byoung Chul Cho [1,8]

To cite: Lee JB, Baek S, Kim DK, *et al*. Phase I trial of CJRB-101 plus pembrolizumab in patients with metastatic non-small cell lung cancer, head and neck squamous cell carcinoma and melanoma. *Journal for ImmunoTherapy of Cancer* 2026;**14**:e014702. doi:10.1136/jitc-2025-014702

► Additional supplemental material is published online only. To view, please visit the journal online (https://doi.org/10.1136/jitc-2025-014702).

Accepted 16 February 2026

For numbered affiliations see end of article.

Correspondence to
Professor Byoung Chul Cho; cbc1971@yuhs.ac

Arim Min; ferix1217@naver.com

ABSTRACT

Background Dysbiosis of gut microbiome leads to resistance to immunotherapy in various advanced solid tumors. CJRB-101 is a live biotherapeutic product consisting of a novel strain belonging to the species *Leuconostoc mesenteroides*. To modulate the tumor microenvironment, CJRB-101 was combined with pembrolizumab.

Methods Preclinical efficacy and mechanistic studies were performed using humanized non-small cell lung cancer (NSCLC) patient-derived xenograft (PDX) models. This is a multicenter, first-in-human, two-part, phase I, open-label study of CJRB-101 (1×10^{11} or 4×10^{11} colony forming unit (CFU)/day) plus pembrolizumab (200 mg every three weeks (Q3W)) in advanced NSCLC, melanoma, and head and neck squamous cell carcinoma in both immune checkpoint inhibitor (ICI)-naive and ICI-refractory settings. The primary endpoint was to assess the dose-limiting toxicities (DLTs), adverse events, and preliminary activity of the combination treatment. Exploratory endpoints included stool metagenomics analysis and pharmacodynamics parameters.

Results In four PDX models, CJRB-101 with pembrolizumab demonstrated enhanced antitumor efficacy, showing a tumor growth inhibition (TGI) of 77.3% in the CJRB-101 monotherapy group and 61.9% in the combination group, which was significantly improved compared with pembrolizumab alone. A distinct M2-to-M1 repolarization was observed and validated in vitro. Notably, increased activation of cytotoxic T cells was observed, suggesting an immune-mediated antitumor mechanism of CJRB-101. A total of 42 patients were enrolled in the low-dose cohort (one capsule once a day; n=6) and high-dose cohort (two capsules two times a day, n=36). Metastatic NSCLC accounted for 86% (n=36) and 67% (n=28) of the patients were refractory to ICIs. None of the patients experienced DLT. In ICI-naïve NSCLC (n=12) with programmed death-ligand 1 (PD-L1) >50%, the overall response rate (ORR) and disease control rate (DCR) were 58% and 75%, respectively. The ORR was 5% and DCR was 41% in the ICI-refractory NSCLC (n=22) with an ORR of 5% and DCR of 41%. After a median follow-up of 15.6 months and 8.9 months for ICI-naïve and ICI-refractory NSCLC, the median progression-free survival was 9 months (95% CI 5.6 to not reached) and 1.8 months (95% CI 1.6 to 4.3), respectively. CJRB-101 plus pembrolizumab was well-tolerated, and none of the patients experienced grade ≥3 treatment-related adverse events.

Conclusions Early clinical data show encouraging antitumor response of CJRB-101 plus pembrolizumab in ICI-naïve metastatic NSCLC with PD-L1 ≥50%.

Trial registration number NCT05877430.

WHAT IS ALREADY KNOWN ON THIS TOPIC

⇒ Only a subset of patients responds to immunotherapy in advanced solid tumors, including non-small cell lung cancer. Modulating the gut microbiome may alleviate resistance to immunotherapy.

WHAT THIS STUDY ADDS

⇒ The trial showed that CJRB-101 plus pembrolizumab yielded an objective response in 58% with progression-free survival of 9 months in immune checkpoint inhibitor (ICI)-naïve metastatic non-small cell lung cancer (NSCLC) with programmed death-ligand 1 ≥50%. CJRB-101 promotes M2-to-M1 macrophage repolarization within the tumor microenvironment and enhances T-cell activation, collectively supporting an antitumor immune response.

HOW THIS STUDY MIGHT AFFECT RESEARCH, PRACTICE OR POLICY

⇒ The addition of CJRB-101 with pembrolizumab resulted in improvement of response rates in ICI-naïve, metastatic NSCLC without actionable genomic alteration. The combination was well-tolerated with no new safety signals observed.

INTRODUCTION

Immune checkpoint inhibitors (ICIs) are pivotal in the treatment landscape for advanced solid tumors, including non-small cell lung cancer (NSCLC), melanoma, and head and neck squamous cell carcinoma (HNSCC).[1] Pembrolizumab, a programmed cell death protein 1 (PD-1) inhibitor, has shown robust antitumor response as monotherapy[2] or combination with platinum doublet chemotherapy[3] in advanced NSCLC without oncogenic driver alterations. Despite the improvement of progression-free survival (PFS) and overall survival (OS), the majority of patients experience disease progression. As the treatment paradigm continues to evolve in metastatic solid tumors, understanding the resistance mechanism and optimizing treatment upfront is paramount in maximizing therapeutic response.

One of the key modulators of tumor microenvironment (TME) is the composition of the gut microbiome.[4] Dysbiosis of the gut microbiome is associated with resistance to ICIs and modulating the gut microbiome via fecal microbiota transplant (FMT) and live biotherapeutic products (LBPs).[5] In patients with advanced melanoma refractory to anti-PD-1 therapy, the addition of FMT to anti-PD-1 resulted in improved clinical benefit (CB).[6]

CJRB-101 is an LBP that contains a novel strain belonging to the species *Leuconostoc mesenteroides* (*L. mesenteroides*), which is a gram-positive, facultative anaerobic, non-spore-forming, and coccus-shaped lactic acid-producing bacteria. *L. mesenteroides* is enriched in dairy products and fermented vegetables such as kimchi. *Leuconostoc* was also enriched in responders to immunotherapy in patients with NSCLC.[7] Previously, preclinical studies have shown that CJRB-101 augments antitumor activity via repolarization of M2 to CXCL9 and CXCL10 dual-expressing M1 macrophages and elicits synergy with pembrolizumab.[8] Preliminary efficacy of CJRB-101 plus pembrolizumab in NSCLC and HNSCC as ICI-naïve and ICI-refractory settings showed promising antitumor response.[9] Here, we report the safety, tolerability and preliminary efficacy of the phase I study of CJRB-101 plus pembrolizumab in patients with advanced NSCLC, HNSCC and melanoma who were ICI naïve and refractory to ICIs. In addition, we provide mechanistic insight to how CJRB-101 modulates the TME and synergizes with pembrolizumab in preclinical models.

METHODS

Efficacy test in syngeneic mouse model

Syngeneic mouse model with C3PQ (lung squamous cell carcinoma) was used for evaluation of the CJRB-101 and anti-PD-1 combination. BALB/C female mice (7 weeks of age) were implanted subcutaneously on the right flank with 1×10^6 syngeneic C3PQ cell line. Procedures involving the care and use of animals in this study were reviewed and approved by the Institutional Animal Care and Use Committee (IACUC number, 2018–0154) before the study. CJRB-101 was administered orally two times a day at 1×10^9 colony-forming unit (CFU). Mouse anti-PD-1 was administrated twice a week at 10 mg/kg (intraperitoneal (i.p.), two times a day). Tumor size was measured daily using vernier calipers. And the equation for tumor volume was "length × width^2 × 0.532". Mice were sacrificed 1 day after the last treatment.

Efficacy test in humanized patient-derived xenograft (PDX) models YHIM-2003, YHIM-2004, YHIM-2009 and YHIM-2014 are PDX models originated from patients with NSCLC who have received a surgical operation in Yonsei Cancer Center. Procedures involving the care and use of animals in this study were reviewed and approved by the IACUC (number, 2022–0041) before the study. Tumor samples were implanted in Hu-CD34-NSG mice or NOG mice. CJRB-101 was administered orally two times a day at 1×10^9 CFU. Pembrolizumab (Keytruda, MSD) was administered once every 5 days at 10 mg/kg (i.p., every five days (Q5D)).

Immune cell depletion assay

Syngeneic mouse model with C3PQ (lung squamous cell carcinoma) was used for evaluation of immune cell depletion under CJRB-101 and anti-PD-1 combination treatment. CJRB-101 and anti-PD-1 were administered following the same dosing schedule used in the efficacy test described above. Cellular subsets were depleted by administering 400 µg/head of antibodies as follows: anti-CD8-α, anti-Ly-6G/Ly-6C two times a week. Macrophages were depleted using 300 µg anti-CD115 every other day. These depletion regimens, including antibody clones, doses, and schedules, were selected based on conditions previously validated in our prior study (PMID: 36545214).

Single-cell RNA sequencing

The tumor samples were dissociated and prepared using single-cell library kits (10x Genomics, 5' end chromium) for single-cell RNA sequencing (scRNA-seq) through Macrogen (Korea). After passing the quality check of complementary DNA, the depth of sequencing read was defined depending on the quality and cell count of cells. Additional sequencing to increase depth was requested after initial inspection of unique molecular identifier (UMI) and read counts. Sequencing data was then processed using the 10x Genomics Cell Ranger V.7.0.1 multi pipeline. The pre-built GRCh38 and mm10 reference transcriptome was used. ScRNA-seq data were analyzed using "Seurat" in R and "Scanpy" in Python. Cells with more than 90% of the human gene abundance, less than 20% of the mitochondrial gene abundance and a minimum of 100 genes were retained, and genes with a minimum of three cells were retained. Cell doublets were identified by "Scrublet" and removed. Cell types were identified by initially mapping single cell profiles to the Azimuth human lung reference V.1, followed by manual re-annotation. For downstream analysis, we used "presto", "dittoSeq" and "EnhancedVolcano" packages in R and Monocle 3. To conduct gene enrichment analysis, we used the ClueGO module in Cytoscape. The

reference database was derived from the Gene Ontology (GO) immune system process, excluding annotations inferred from electronic sources. The parameters were set as follows: the threshold for the minimum number of genes in each term was set at 3, and the GO tree interval was defined within a range from 3 to 8. Statistical options included enrichment/depletion using a two-sided hypergeometric test, and Benjamini-Hochberg correction was applied for multiple comparisons.

Immune profiling using flow cytometry analysis

Tumor cells collected from in vivo models were enzymatically dissociated into single cells with mechanical, enzymatical dissociation systems. Tumors were cut into small fragments 2–4 mm in length and put in gentleMACS C-tube containing the enzyme mixture. Tumor fragments and the enzyme mix were dissociated using the gentleMACS dissociator and incubated for 30 min at 37°C under continuous rotation. This step was repeated three times with different gentleMACS dissociator programs. Then filtered through a 70 µm cell strainer. Mouse intestines were dissociated using Lamina propria dissociation kit and gentleMACS dissociator. Isolated cells were stained with target-specific antibodies and subsequently analyzed by flow cytometry. Multicolor flow cytometry analysis was performed using a BD LSRFortessa X-20 instrument. FlowJo software V.10 was used for data acquisition and analysis.

Multiplexed iImmunohistochemistry

For the multiplexed immunohistochemical staining of the sections, BOND RX Fully Automated Research Stainer was used and an Opal Polaris 7 Color IHC Detection Kit. All procedures were performed according to the manufacturer's instructions. Multiple staining rounds were performed using the following anti-human antibodies: anti-CD68, anti-PD-L1, anti-granzyme B, anti-CD16, anti-CD11c, anti-CD4, anti-CD8, anti-PD-1, anti-FoxP3 and anti-PanCK. Tissue sections were counterstained with Spectral DAPI.

Imaging analysis

Images of the whole tissue contents were generated using whole-slide scanning by using Vectra Polaris Automated Quantitative Pathology Imaging System. Multispectral images for analysis were defined and selected within the whole tissue using Phenochart whole slide contextual viewer software. The inForm software, equipped with an integrated algorithm for tissue analysis, was employed to transform the multispectral image data into numerical data. These data encompassed both numerical and spatial information regarding the tumor nest and stromal region, defining the cell components (nuclear, cytosolic, and membrane margins), classifying the cell populations and the intensities of each marker. Cell populations were discerned based on the distinctive patterns of CD marker expression, each exhibiting unique cellular properties, such as nuclear, cytosolic, and membranal sizes and shapes (CD4 and CD8 for T cells, CD68 for macrophages, Pan-CK for epithelial cells or cancer cells and FoxP3 for regulatory T cells (Treg)). The differentiation between the tumor nest and stroma, as well as the area calculations, was done based on the pan-cytokeratin staining patterns by using an algorithm integrated into the inForm software. The integrated matrix files were derived from the segmentation of cells and tissues from the tissue microarray (TMA) data. These data included the fluorescence intensity in the nucleus and cytosol. The extracted CSV file was converted into an FCS file using the R program. The FCS file was subsequently converted into a raw file for cytometric image analysis using FlowJo.

BMDM repolarization assay

Bone marrow was collected from the tibia and femur of female C57BL/6N mice, and marrow cells were flushed with RPMI containing 10% fetal bovine serum (FBS) and 1% penicillin–streptomycin. After centrifugation, cells were subjected to red blood cell (RBC) lysis for 2 min, washed, resuspended in complete RPMI, and filtered through a 100 µm strainer. A total of 8×10^6 bone marrow cells were plated per 10 cm dish and differentiated into bone marrow-derived macrophages (BMDMs) in RPMI supplemented with 10% FBS, 1% penicillin–streptomycin, and macrophage colony-stimulating factor (M-CSF) (10 ng/mL). Fresh M-CSF–containing medium was supplied on day 4, and cells were further cultured for an additional 3 days. Differentiated BMDMs were seeded at 1×10^5 cells per well in 24-well plates and rested for 24 hours. For polarization, BMDMs were incubated with dexamethasone (100 nM) in M-CSF–containing medium for 24 hours, followed by treatment with CJRB-101 (BMDM:bacteria ratio 1:10) or CJRB-101 cell membrane (CM), cell wall, lipoteichoic acid, lipoprotein fraction (10–100 µg/mL) for 24 hours. Macrophage phenotype was analyzed by flow cytometry using anti-EMR1, anti-IA/IE, and anti-CD206 antibodies to assess M1 and M2 populations.

Immune profiling using flow cytometry analysis

After anti-PD-1 and CJRB-101 combination treatment, organs were sampled at each time point (day 3, 7, 10, end of timepoint (EOT)). Tumor tissues were obtained to confirm the immune population that most affects the antitumor effect in the TME, and gut (jejunum, colon) was obtained for local immune population. In addition, the spleen was collected for system immunity. The organs and tumor tissues were dissociated using gentleMACS dissociator and analyzed using flow cytometry.

Isolation of cell membrane fraction

Bacterial pellet was resuspended in 0.1 M sodium citrate buffer (pH 4.7) and disrupted by ultrasonication (Vibracell VCX500; Sonics and Materials, Newtown, Connecticut, USA) with stirring on ice for 90 min. The bacterial lysates were mixed with an equal volume of n-butanol and the aqueous phase (lower phase) was

collected by centrifugation at 13,000 g for 15 min. The collected aqueous phase was then dialyzed through a dialysis membrane (Spectrum Laboratories, Rancho Dominguez, California, USA) against sterile water (Daihan Pharm, Seoul, Korea) at 4°C for 72 hours, changing with new sterile water three times a day. The cell membrane fraction was lyophilized and then the quantity was determined by measuring the dry weight.

Macrophage-mediated activation of T-cell cytotoxicity assay

CT26 subcutaneous tumors were minced and enzymatically dissociated in RPMI supplemented with 2% FBS, 0.01 mg/mL DNase I, and 400 U/mL Collagenase IV using a gentleMACS system at 37°C for 1 hour, followed by filtration through a 70 µm strainer and RBC Lysis. Tumor-associated macrophages (TAMs) were purified as $F4/80^+$ cells using anti-F4/80 MicroBeads (Miltenyi). Splenocytes from C57BL/6 mice were obtained by collagenase-assisted flushing of the spleen, incubated for 25 min at 37°C. Naïve $CD8^+$ T cells were purified using a Miltenyi naïve $CD8^+$ T-cell isolation kit. For co-culture, 24-well plates were coated with anti-CD3 (0.1 µg/mL), and CT26 cells (1×10^4) were cultured with $CD8^+$ T cells in the presence of soluble anti-CD28 (1 µg/mL), mIL-2 (30 U/mL), and IFN-γ (10 ng/mL). Purified TAMs (5×10^4) were placed in 0.4 µm transwell inserts and stimulated with CJRB-101 CM fraction (100 µg/mL) and M-CSF (10 ng/mL), maintaining a cancer:TAM:T-cell ratio of 1:5:25. Supernatants were collected after 24 hours for CXCL9 quantification, and CT26 cell viability was analyzed after 48 hours by flow cytometry using Fixable Viability Stain 510.

Statistical analysis in preclinical studies

Data are presented as mean±SEM. Statistical analyses were performed using GraphPad Prism V.10.0 (GraphPad Software) and R software. Prior to parametric testing, data distribution was assessed for normality. Flow cytometry data were analyzed using unpaired two-tailed Student's t-tests. Comparisons among multiple groups were conducted using one-way or two-way analysis of variance, as appropriate, followed by post hoc multiple-comparison tests when applicable. Correlation analyses were performed using Pearson's correlation coefficient. For in vivo experiments, statistical analyses were performed with a minimum sample size of n=3 per group, while in vitro experiments were conducted with at least three independent biological replicates. A p value<0.05 was considered statistically significant.

Study design and patients

This study (NCT05877430) was a multicenter, FIH, 2-part, phase I, open-label study that evaluated CJRB-101 plus pembrolizumab in patients with advanced and metastatic NSCLC, HNSCC, and melanoma who were either ICI-naïve or refractory to ICIs. Part 1 consisted of a lead-in phase with six patients allocated to low dose (one capsule once a day) and six patients in high dose (two capsules two times a day) followed by part 2 of dose exploration (N=30) that only included high dose of CJRB-101.

Details to full eligibility are provided in the study protocol as online supplemental file 1. Patients with histologically or cytologically confirmed stage IV NSCLC, HNSCC, and melanoma who were ICI-naïve and refractory to ICIs were included. In NSCLC, patients were eligible only if they were negative for *EGFR* and *ALK*. Key inclusion criteria of programmed death-ligand 1 (PD-L1) expression differed across tumor cohorts. For the ICI-naïve cohort, PD-L1 tumor proportion score ≥50% and combined positive score ≥20 for NSCLC and HNSCC, respectively, were enrolled. In the ICI-refractory cohort, patients were enrolled regardless of PD-L1 expression. ICI-refractory was defined as progression after at least two cycles of anti-PD-(L)1 therapy either as monotherapy or combination as per the Response Evaluation Criteria in Solid Tumors (RECIST) V.1.1, and patients with NSCLC or HNSCC who progressed with platinum-based chemotherapy were eligible. Patients who received less than three of systemic therapy were included in the ICI-refractory cohort. Patients with Eastern Cooperative Oncology Group performance status of 0 or 1, and able to ingest capsules, were included.

Treatment

In part 1 of the lead-in phase, six patients were initially treated with CJRB-101 (1×10^{11} CFU/day) at low dose (one capsule once a day) before proceeding with high dose (two capsules two times a day, 4×10^{11} CFU/day) in with part 1 and part 2 of dose exploration phase. Pembrolizumab was given intravenously at 200 mg of each 21-day cycle.

Assessments

In part I, patients were followed for 21 days after the first dose of treatment for the occurrence of dose-limiting toxicities (DLTs) (Data). Enrollment to part 2 was permitted only if less than three DLTs occurred in six patients.

CT and MRI scans were performed at baseline and every 8 weeks for the first 6 months followed by every 12 weeks until investigator-assessed disease progression, consent withdrawal or death. The severity of adverse events (AEs) was measured using the National Cancer Institute Common Technology Criteria for Adverse Events V.5.0. Patients were continuously monitored for AEs during treatment and 6 weeks after last treatment.

PD-L1 was tested using immunohistochemistry 22C3 pharmDx (Agilent Technologies, Carpinteria, California, USA). Fecal and blood samples for pharmacodynamic analysis were collected on or within 7 days before Cycle 1 day 1, Cycle 2 day 1, during every CT and MRI scan, and at end of treatment.

Taxonomic profiling of stool samples

Stool samples were collected from patients for both shotgun and amplicon sequencing. For shotgun

sequencing, the sequencing libraries were prepared according to the manufacturer's instructions for the TruSeq Nano DNA High Throughput Library Prep Kit (Illumina). Sequencing was performed by Macrogen using the NovaSeq X (Illumina). For amplicon sequencing, the sequencing libraries were prepared following the Illumina 16S Metagenomic Sequencing Library protocol to amplify the V3–V4 region of the 16S rRNA gene. Sequencing was performed by Macrogen using either the MiSeq (Illumina) or the MiSeq i100 (Illumina).

Shotgun sequencing data were taxonomically profiled using the EzMx platform.[10] The potential presence of bacterial and archaeal species in each shotgun sequencing dataset was assessed using Kraken2[11] and a pre-built core gene database,[12] which contains k-mers (k=35) derived from reference genomes obtained from the EzBioCloud database.[10] Subsequently, each shotgun sequencing dataset was mapped against a custom Bowtie2 database,[13] constructed using core genes and genomes from species identified in the previous step. SAMtools[14] was used to convert and sort the resulting BAM files, and BEDTools[15] was employed to determine the coverage of mapped reads.

Microbial diversity was determined using amplicon sequencing data processed with QIIME2 (V.2022.11).[16] Primer sequences were trimmed with the cutadapt plugin,[17] and untrimmed reads were discarded. Paired-end reads were processed and denoised with the dada2 plugin.[18] The resulting amplicon sequence variants were classified against the EzBioCloud database[10] using the classify-consensus-vsearch pipeline with a 97% identity threshold and 80% coverage.[19 20] All statistical analyses and visualizations were carried out using R. Wilcoxon rank-sum test or Wilcoxon signed-rank test was used for statistical analyses.

Endpoints

The primary endpoint of part 1 and 2 was to determine the DLTs and AEs of CJRB-101 with pembrolizumab in patients with advanced or metastatic NSCLC, HNSCC, and melanoma. The secondary endpoints were overall response rate (ORR), disease control rate (DCR), duration of response and PFS. Exploratory endpoints included pharmacodynamics markers in blood and baseline tumor samples, and fecal microbiota and metagenomics analysis of taxonomic composition.

Statistical analysis in clinical studies

Efficacy and safety were assessed in all patients who received at least one dose of CJRB-101 plus pembrolizumab. PFS was estimated using the Kaplan-Meier method. All analysis was performed using R.

Data availability

Processed data, including Seurat objects for scRNA-seq that were used to generate the figures in this manuscript, have been deposited at figshare and are publicly available at https://doi.org/10.6084/m9.figshare.30969202 as of the date of publication. All original code for scRNA-seq analyses has been deposited at GitHub and is publicly available at https://github.com/Hyun7564/CJRB-101 as of the date of publication.

RESULTS

CJRB-101 demonstrates immune-driven antitumor effects in lung cancer syngeneic mouse models and humanized NSCLC patient-derived xenograft models.

First, we evaluated the antitumor efficacy of the anti-PD-1 and CJRB-101 combination in the C3PQ syngeneic model. CJRB-101 monotherapy and CJRB-101 and anti-PD-1 combination treatment significantly suppressed tumor growth compared with anti-PD-1 alone (figure 1A).

To define the immune populations responsible for this activity, depletion studies were performed in the C3PQ model (figure 1B). Loss of $CD8^+$ T cells, neutrophils/monocytes, or macrophages all abrogated the antitumor effect, and survival was correspondingly reduced in each depletion group (figure 1C). These findings indicate that $CD8^+$ T cells, macrophages, and neutrophils are essential mediators of the therapeutic response elicited by CJRB-101 in combination with anti-PD-1.

To investigate how orally administered CJRB-101 links immune responses from the gut to the tumor microenvironment, we performed Gut–TME axis immune profiling. Early after treatment, macrophages and natural killer (NK) cells increased in the jejunum and colon, followed by systemic $CD8^+$ T-cell activation in the spleen and subsequent accumulation within tumors. Together, these findings support a coordinated and temporally ordered immune response, in which early gut-resident innate immune activation is associated with subsequent systemic and intratumoral $CD8^+$ T-cell expansion, consistent with a model of immune coordination contributing to tumor control (online supplemental figure 1AB).

Given this strong immune-mediated activity in syngeneic models, we next examined efficacy in humanized PDX models.

CJRB-101 was tested across multiple NSCLC PDX models (YHIM-2003, YHIM-2004, YHIM-2009 and YHIM-2014) engrafted into Hu-CD34-NSG mice. As part of model characterization, the range of responsiveness to immune checkpoint blockade was first evaluated; their sensitivity to anti-PD-L1 antibody (durvalumab) is provided in online supplemental Figure 2A-C. Notably, the YHIM-2004 model showed a moderate response to pembrolizumab and was therefore selected for subsequent mechanistic studies.[21]

In the high-dose CJRB-101 monotherapy group, 77.3% of mice achieved >50% tumor growth inhibition (TGI), while 61.9% exceeded this threshold in the combination group. In contrast, only 23.8% of pembrolizumab monotherapy mice reached >50% TGI, representing the weakest response (figure 1D).

Collectively, these results demonstrate that CJRB-101, administered either as a monotherapy or in combination

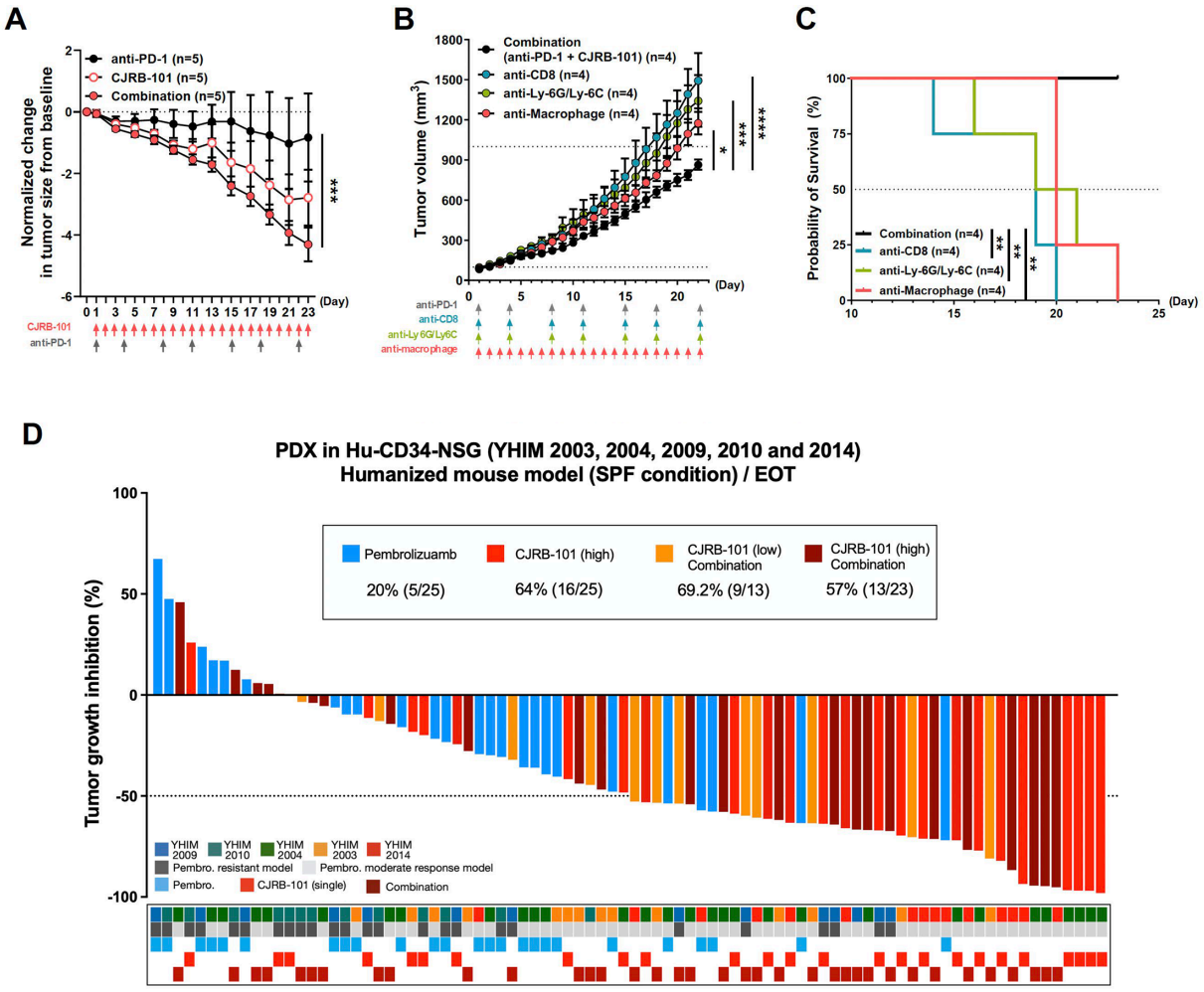

Figure 1 CJRB-101 demonstrates immune-driven antitumor effects in syngenetic mouse models and humanized NSCLC patient-derived xenograft models. (A) Normalized change in tumor volume from baseline in C3PQ syngeneic model. (B) Tumor volume and (C) probability of survival (%) of immune cell ($CD8^+$ T cell, Ly-6G/Ly-6C, Macrophage) depletion assay in C3PQ syngeneic model. (D) Waterfall plot of tumor growth inhibition (%) across four NSCLC humanized PDX models. NSCLC, non-small cell lung cancer; PD-1, programmed cell death protein 1; PDX, patient-derived xenograft.

with pembrolizumab, consistently produced stronger antitumor responses than pembrolizumab monotherapy across four NSCLC PDX models (YHIM-2003, YHIM-2004, YHIM-2009, YHIM-2014). Importantly, we observed clear tumor growth inhibition in the pembrolizumab-resistant model YHIM-2009. Tumor volume results for each PDX model are provided in the online supplemental Figure 2D-G.

CJRB-101 was evaluated across multiple PDX models, and its activity was confirmed to be immune mediated, as antitumor effects were observed in Hu-CD34-NSG mice but not in immune-deficient NOG mice (online supplemental Figure 2H and I).

Enhanced antitumor efficacy of CJRB-101 combined with pembrolizumab through myeloid-cell-mediated immune activation.

Tumor tissues from the YHIM-2004 humanized PDX model were comprehensively analyzed for immune profiling using scRNA-seq, flow cytometry (FACS), and multiplex immunohistochemistry (IHC). For scRNA-seq analysis, the myeloid and T/NK compartments were separated and analyzed independently. In the myeloid compartment analysis, trajectory analysis revealed that CJRB-101 treatment induced a progressive transition from M2-like macrophages toward an M1-polarized state. This M2-to-M1 repolarization was further supported by uniform manifold approximation and projection (UMAP) feature plots, which showed distinct distributions of M1-associated and M2-associated gene set module scores along the trajectory (online supplemental Figure 3A and online supplemental table 1). Along this differentiation trajectory, CXCL9 and CXCL10 expression progressively increased with pseudotime, aligning with the acquisition of pro-inflammatory M1 characteristics (figure 2A and B). Consistent with these findings, feature plots demonstrated a marked induction of CXCL9 and CXCL10 within this macrophage subset (online supplemental Figure 3B). In line with this, the M2-to-M1 repolarized macrophage population was diminished by pembrolizumab monotherapy. However, this population was increased with CJRB-101 monotherapy and combination treatment (figure 2C). Flow cytometry analysis revealed a significant

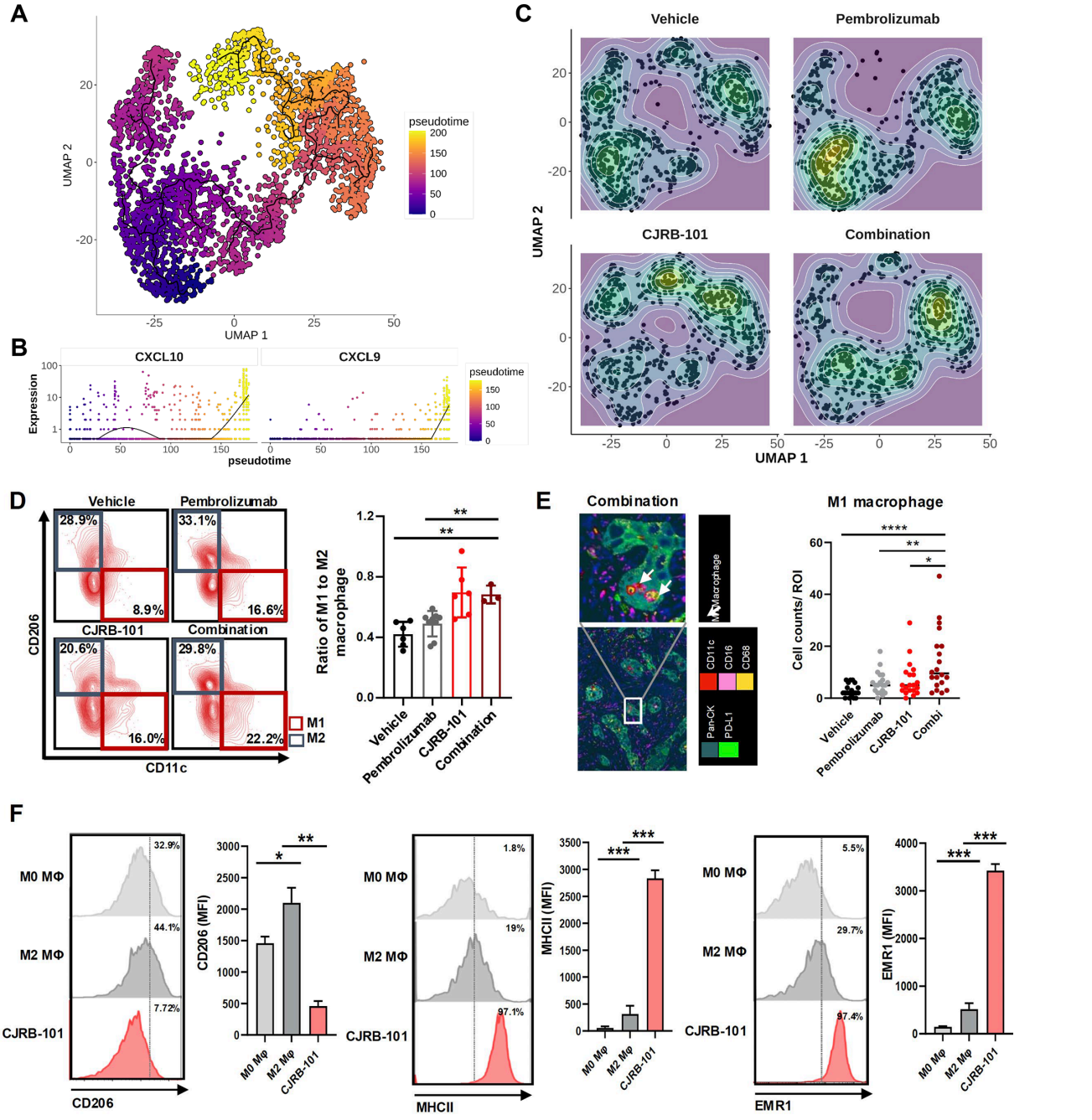

Figure 2 Enhanced antitumor efficacy of CJRB-101 combined with pembrolizumab through myeloid-cell-mediated immune activation. (A) Trajectory analysis showed that CJRB-101 induced repolarization of M2 to M1 macrophages. (B) Population of CXCL9^{+}CXCL10^{+} M1 macrophages across treatment groups. (C) Trajectory analysis showing the pseudotime-dependent increase of CXCL9 and CXCL10 expression along the macrophage differentiation axis. (D) Macrophage polarization reflected by the M1/M2 ratio by FACS analysis. (E) Multiplex IHC-based comparison of intratumoral M1 macrophage infiltration across groups. (F) M1 polarization and M2 to M1 repolarization induced by CJRB-101 in BMDM. BMDM, bone marrow-derived macrophages; FACS, flow cytometry; IHC, immunohistochemistry; UMAP, uniform manifold approximation and projection.

increase in the M1/M2 macrophage ratio in the combination group (figure 2D). Consistently, multiplex IHC demonstrated significantly enhanced infiltration of M1 macrophages (CD11c^{+}CD68^{+}) into the TME in the combination group (figure 2E). To determine whether CJRB-101 directly induces macrophage repolarization, an in vitro BMDM repolarization assay was performed. After differentiating BMDMs into M2 macrophages, treatment with CJRB-101 resulted in a significant upregulation of the M1 markers MHC-II and EMR1, accompanied by a significant reduction in the M2 marker CD206 (figure 2F). To identify the active component of CJRB-101, we performed cell fractionation and found that the CM fraction was an effective molecule (online supplemental Figure 4A and B and online supplemental Figure 5). We further examined CJRB-101 CM–induced macrophage

repolarization and found that TLR4 inhibition substantially attenuated CJRB-101 CM–driven M2 to M1 repolarization. These findings indicate that CJRB-101 CM mediates macrophage reprogramming through a TLR4-dependent pathway. CJRB-101 CM recapitulated the antitumor efficacy observed with CJRB-101 in the C3PQ model. Inhibition of TLR4 subsequently attenuated the CJRB-101 induced enhancement of antitumor activity. We confirmed that the CJRB-101 CM-mediated antitumor activity is dependent on TLR4 signaling in both in vitro and in vivo settings (online supplemental Figure 6A and B). Taken together, CJRB-101 drives macrophage polarization toward an M1 phenotype and promotes the repolarization of M2 to M1 macrophages, thereby enhancing macrophage-mediated antitumor activity. This represents a distinctive mechanistic feature of CJRB-101.

Enhanced antitumor efficacy of CJRB-101 combined with pembrolizumab through expansion of central memory T cells and increased T-cell cytotoxic activity.

In the T/NK compartment, subclustering based on canonical marker genes revealed that central memory T cell (Tcm) and NK-associated clusters were enriched in the combination group compared with the pembrolizumab group (figure 3A and B and online supplemental Figure 7). Differential expression analysis between the two groups further supported these findings. Combination with CJRB-101 exhibited elevated expression of cytotoxic effector molecules (GZMB, PRF1, GLNY) and activation receptors (TNFRSF18, CXCR6), whereas pembrolizumab monotherapy was characterized by higher expression of Treg-associated genes such as CTSC and FOXP3 (figure 3C). These transcriptional differences are consistent with the reduced Treg proportion observed in the combination group. GO pathway enrichment analysis based on differentially expressed genes demonstrated that combination was associated with pathways related to NK-cell and T-cell activation, while pembrolizumab monotherapy showed enrichment of pathways linked to Treg differentiation (figure 3D). Consistent with the scRNA-seq findings, there was a significant increase in tumor-infiltrated Tcm cells in the combination group in the FACS analysis (figure 3E). In addition, the cytotoxic effector molecule interferon-γ was significantly upregulated in tumor-infiltrating $CD8^+$ T cells in the combination group (figure 3F). Multiplex IHC revealed a significant increase in both Granzyme B^+ cytotoxic T cells (Tc) and Granzyme B^+ helper T cells (Th) within the tumor site (figure 3G). Treatment with CJRB-101 resulted in increased intratumoral Tcm cells and expression of cytotoxic molecules, collectively supporting its contribution to enhanced antitumor activity.

Patient disposition and baseline characteristics

The first patient was dosed on October 13, 2023, in part 1 of the lead-in phase and the last patient was dosed on March 5, 2025, in part 2 of the dose exploration phase. An overview of the patient disposition is included in the consort diagram (online supplemental Figure 8). At the time of data cut-off (October 27, 2025), 42 patients from South Korea and the USA were enrolled, including 12 patients (low dose, n=6; high dose, n=6) in part 1 and 30 patients in the high dose in part 2 dose exploration phase. The median age was 67 years (IQR 62–73), and most of the patients were Asian (88%, n=37) (online supplemental Table 2). Metastatic NSCLC accounted for 86% (n=36) and 67% (n=28) of the patients were refractory to ICIs, of which 64% (n=18) were treated as second-line therapy.

DLTs and safety overview

None of the patients experienced DLTs with both low dose and high dose of CJRB-101 in combination with pembrolizumab in all cohorts. Additional safety data are summarized in online supplemental Tables 3 and 4. The most common treatment-related adverse events (TRAEs occurring in >5% of patients) were aspartate aminotransferase (AST) (n=4, 10%) and alanine aminotransferase (ALT) elevation (n=4, 10%), and diarrhea (n=3, 7%) of grade 1–2. The combination treatment was well tolerated with no grade ≥3 TRAEs (online supplemental Table 5-7). There was no dose reduction, interruption, or discontinuation of treatment due to CJRB-101 or pembrolizumab.

Efficacy overview

39 patients (ICI-naïve, n=13, ICI-refractory, n=26) had imaging studies evaluable for efficacy analysis (online supplemental Figure 9). The ORR was 58% and DCR was 75% for the ICI-naïve NSCLC (n=12) (figure 4A), with four patients ongoing at the time of data cut-off (figure 4B). At median follow-up duration for 15.6 months (95% CI 11.1 to not reached (NR)), the median PFS was 9 months (95% CI 5.6 to NR) (online supplemental Figure 10). In patients with metastatic NSCLC (n=22) who were refractory to ICI, the ORR and DCR were 5% and 41%, respectively. The antitumor activity of the combination is shown in the spider plot (online supplemental Figure 11). The median follow-up was 8.9 months (95% CI 8.2 to NR), and median PFS was 1.8 months (95% CI 1.6 to 4.3). In the ICI-naïve HNSCC cohort (n=3), one patient remains with stable disease for 12 months. All patients in the ICI-refractory cohort of HNSCC (n=2) and melanoma (n=2) experienced disease progression after two cycles of treatment.

Stool metagenomics analysis

In ICI-refractory patients, microbial diversity was significantly lower in baseline stool samples of patients with CB (defined as partial response or stable disease) compared with those with no clinical benefit (NCB defined as progressive disease) (observed species, p=0.025; Shannon index, p=0.027) (figure 4C). In both ICI-naïve (n=14) and ICI-refractory (n=27) patients, the administration of CJRB-101 resulted in enrichment of *L. mesenteroides* at week 3 and in following weeks in the stool samples (figure 4D). The relative abundance of *L. mesenteroides* remained elevated in a dose-dependent manner. Furthermore,

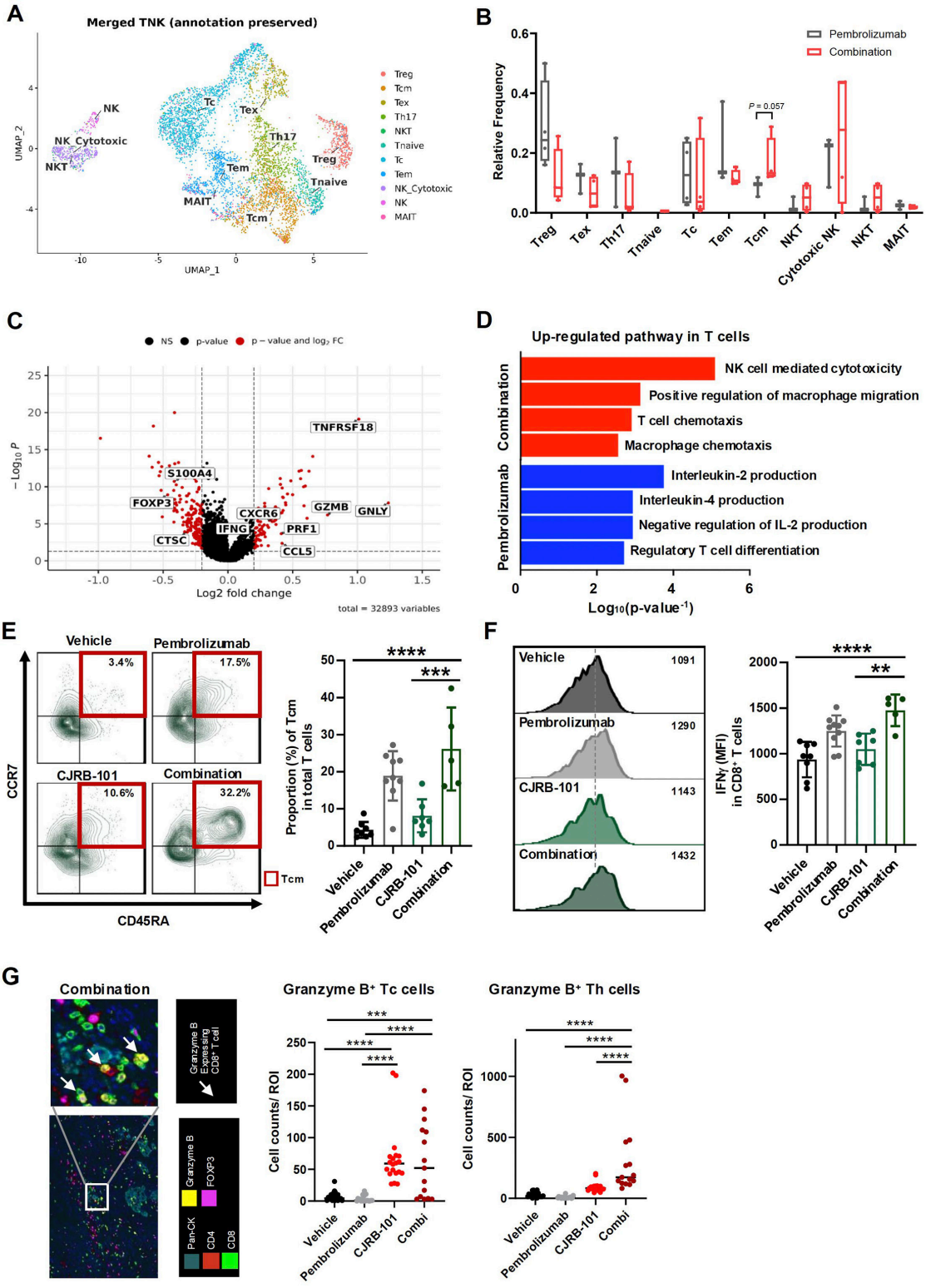

Figure 3 Enhanced antitumor efficacy of CJRB-101 combined with pembrolizumab through expansion of central memory T cells and increased T-cell cytotoxic activity. (A) UMAP visualization of T/NK cell clustering. (B) Comparison of T/NK cell frequencies across pembrolizumab and combination groups. (C) Volcano plot highlighting genes enriched in the combination group. (D) Pathways significantly enriched in the pembrolizumab and combination treatment groups. (E) Flow cytometric evaluation of central memory T-cell frequencies across treatment groups in humanized YHIM2004 PDX tumors. (F) Flow cytometric evaluation of IFN-γ^+ $CD8^+$ T cells across treatment groups in humanized YHIM2004 PDX tumors. (G) Multiplex IHC-based comparison of intratumoral $GzmB^+$ $CD8^+$ and $GzmB^+$ $CD4^+$ T-cell infiltration across groups. IFN, interferon; IHC, immunohistochemistry, MAIT, mucosal-associated invariant T cell; MFI, median fluorescence intensity; NK, natural killer; PDX, patient-derived xenograft; ;Tcm, central memory T cell; Tem, effector memory T cell; Tex, exhausted T cell; Tc cytotoxic T cell; Treg, regulatory T cell.

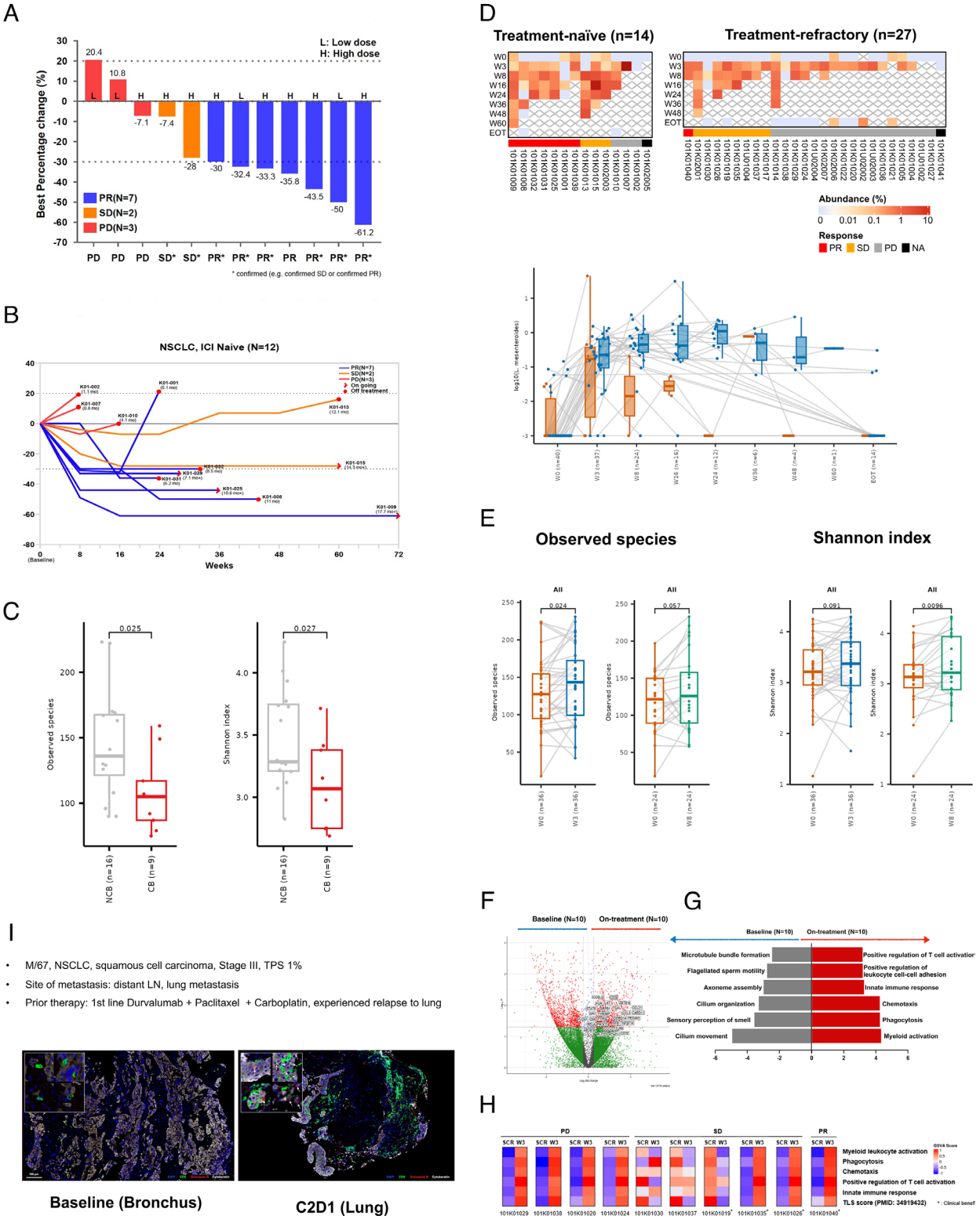

Figure 4 Waterfall plot of ICI-naïve metastatic NSCLC (n=12) (A), spider plot of ICI-naïve metastatic NSCLC (n=12) (B), Comparison of microbial diversity at baseline in ICI-refractory patients (C), relative abundance (%) of *Leuconostoc mesenteroides* in stool samples (D), Microbial diversity increased after administration of CJRB-101 (E), volcano plot of differentially expressed genes comparing baseline (N=10) and on-treatment (N=10) samples (F), and enriched pathways identified by Gene Set Enrichment Analysis (G), changes of patient-specific GSVA score in immune-related pathways between screening and week 3 across PD, SD, and PR groups (H), Multiplex IHC of a patient who achieved disease stabilization for >10 months (I). CB, clinical benefit; EOT, end of timpoint; GSVA, gene set variation analysis; ICI, immune checkpoint inhibitor; IHC, immunohistochemistry; LN, lymph node; NCB, no clinical benefit; NSCLC, non-small cell lung cancer; PD, progressive disease; PR, partial response; SCR, screening; SD, stable disease; TILs, tumor infiltrated lmyphocytes; TPS, tumor proportion score.

microbial diversity increased from baseline after CJRB-101 administration at week 3 (observed species, p=0.024; Shannon index, p=0.091) and week 8 (observed species, p=0.057; Shannon index, p=0.0096) across all patients (figure 4E). At week 3, butyrate-producing bacteria such as *Faecalibacterium, Butyricimonas, Pseudoflavonifractor,* and *Oscillibacter* were enriched after CJRB-101 was administered (online supplemental Figure 12).

Pharmacodynamic effects of CJRB-101 plus pembrolizumab

In ICI-refractory patients, we observed a significant on-treatment upregulation of genes involved in adaptive and innate immune activation and recruitment, including *CCL5, CCL21, TYROBP, IRF8, TLR9,* and *CD3E* (figure 4F). Consistently, gene set enrichment analysis (GSEA) demonstrated marked enrichment of T-cell activation, innate immune responses, and chemotaxis pathways in on-treatment samples, confirming these findings as pharmacodynamic effects (figure 4G and H). A similar increase in immune-activation signatures was also detected in on-treatment samples from the ICI-naïve patient (online supplemental Figure 13). Notably, spatial profiling of tumor tissue from a patient who achieved >10 months of disease stabilization revealed enhanced GZB^+CD8^+ T-cell enrichment and activation following CJRB-101 plus pembrolizumab treatment (figure 4I). In the peripheral blood mononuclear cell (PBMCs), $PD\text{-}1^+TIM\text{-}3^+$ T cells showed a significant reduction that was maintained longitudinally, and the CB group exhibited a marked decrease in polymorphonulcear myeloid-derived suppressor cells (PMN-MDSC) (%) and neutrophil (%), in contrast to the NCB group (online supplemental Figure 14 and online supplemental Figure 15).

DISCUSSION

Currently, treatment options remain limited after progression with ICIs in advanced solid tumors such as NSCLC, HNSCC and melanoma. Resistance mechanisms to immunotherapies have been heterogeneous, and various agents including LBPs have been developed to restore the TME to immune-inflamed status. CJRB-101 was combined with pembrolizumab to overcome the limitations of anti-PD-1 inhibitors given as monotherapy.[22–24] This rationale was supported by preclinical studies showing that CJRB-101 modulates the TME by inducing M2-to-M1 macrophage repolarization and enhancing $CD8^+$ cytotoxic T-cell activation, leading to sustained antitumor activity. In vitro macrophage–T-cell co-culture assays further demonstrated macrophage-mediated activation of T-cell cytotoxicity, supporting the immunostimulatory network induced within the TME. In addition, the CM isolated from CJRB-101 recapitulated the antitumor activity of the live strain, and further purification and mechanism studies aimed to identify the active molecular components are ongoing (online supplemental Figures 5 and 6).

Although our study included patients with HNSCC and melanoma, most of the patients enrolled in this study were treatment-naïve NSCLC with PD-L1 expression of >50%. Current treatment guidelines recommend anti-PD-1 inhibitors as monotherapy or in combination with cytotoxic chemotherapy for patients without actionable genetic alterations and with PD-L1 expression of ≥50%.[25] Our study showed that the addition of CJRB-101 to pembrolizumab in treatment-naïve NSCLC with PD-L1 expression of ≥50% resulted in an ORR of 58% which is numerically higher compared with pembrolizumab monotherapy (44.8%) in the pivotal KEYNOTE-024 study.[2]

Despite the added benefit in terms of numerical increase in response rate for ICI-naïve metastatic NSCLC, marginal benefit was observed across ICI-refractory cohorts (NSCLC, ORR 5%; HNSCC and melanoma 0%). In the future, understanding the mechanism of resistance to ICI in the perspective of gut microbiome is paramount in identifying patients who benefit from subsequent therapies.

Modulating the gut microbiome has been a challenge due to differences in diet composition across ethnicities, resulting in various reports of specific strains being associated with responses to immunotherapy.[4] Although FMTs have shown clinical activity in ICI-refractory melanoma in a subset of patients,[6] the process is not easily applicable and reproducible in the clinical settings. To this end, various LBPs focusing on a specific strain have been developed, but the robustness of clinical activity remains arbitrary. Currently, the focus has shifted from identifying a specific strain to changes in microbial diversity in gut microbiome, which adds complexities to pinpointing the role of gut microbiome in resistance mechanisms to immunotherapy.

In our study, stool metagenomics analysis revealed that the amount of *L. mesenteroides* increased after administration of CJRB-101 plus pembrolizumab. These changes were consistently observed in the following weeks in a subset of patients. Furthermore, CJRB-101 resulted in microbial diversity and butyrate-producing bacteria increased from baseline.

CJRB-101 originates from a food, kimchi, supporting a favorable safety profile and enabling a convenient oral capsule formulation that offers practical advantages over FMT. Although exploratory endpoints such as stool metagenomics analysis were conducted to delineate patient-selection and rationalization for the addition of CJRB-101 to pembrolizumab in treatment-naïve NSCLC with PD-L1 expression of ≥50%, we did not identify robust patient-selection tools. Considering that diet, antibiotics, and probiotics may modulate the gut microbiome, further extensive studies should be carried out prior to generalization of *L. mesenteroides* as therapeutic response to treatment.

Notably, CJRB-101 was well-tolerated with no grade 3 treatment-related toxicities and can be safely administered with pembrolizumab. However, the few toxicity

profiles observed in the study, such as AST/ALT increase and diarrhea of grade 1 and 2.

Limitations include the limited number of sample size enrolled for ICI-refractory HNSCC and melanoma for further investigation. None of the patients with melanoma were recruited in the ICI-naïve cohort. Hence, whether the combination of CJRB-101 plus pembrolizumab augments the antitumor activity seen in NSCLC is similarly observed in melanoma remains unknown.

Overall, the addition of CJRB-101 with pembrolizumab resulted in improvement of response rates in ICI-naïve, metastatic NSCLC without actionable genomic alteration and with PD-L1 expression of ≥50%. The combination was well-tolerated with no new safety signals observed.

Author affiliations
[1]Department of Internal Medicine and Yonsei Cancer Center, Severance Hospital, Yonsei University College of Medicine, Seoul, Korea (the Republic of)
[2]Severance Biomedical Science Institute, Yonsei University College of Medicine, Seoul, Korea (the Republic of)
[3]Brain Korea 21 PLUS Project for Medical Science, Yonsei University College of Medicine, Seoul, Korea (the Republic of)
[4]CJ Bioscience, Inc, Seoul, Korea (the Republic of)
[5]Division of Hematology-Oncology, Department of Medicine, Samsung Medical Center, Sungkyunkwan University School of Medicine, Jongno-gu, Seoul, Korea (the Republic of)
[6]Division of Hematology-Oncology, University of California Irvine School of Medicine, Irvine, California, USA
[7]Department of Medicine and UPMC Hillman Cancer Center, University of Pittsburgh, Pittsburgh, Pennsylvania, USA
[8]Yonsei New Il Han Institute for Integrative Lung Cancer Research, Yonsei University College of Medicine, Seoul, Korea (the Republic of)

Acknowledgements We thank CJ Bioscience company for providing the CJRB-101.

Contributors JBL, SB, DKK, and BEK contributed equally to this work. AM and BCC conceived and supervised the study and are responsible for the overall study design. JBL, SB, DKK, and BEK performed the preclinical experiments and analyzed the data. HP, HK, JI, JY, EY, GHS, SC, JEK, JMK, SYK, HSO, MC, and AM contributed to immune profiling, mechanistic analyses, and data interpretation. YK, SYP, JHK, and DKK contributed to data curation and statistical analyses. JSA, MN, and DD contributed to clinical data acquisition and interpretation. JBL, SB, DKK, and BEK drafted the manuscript. Guarantor: AM and BCC accept full responsibility for the work and/or the conduct of the study, had access to the data, and controlled the decision to publish. All authors critically reviewed, edited, and approved the final version of the manuscript. AI (Chat-GPT)-assisted technologies were used only for language editing and readability enhancement.

Funding This work was supported by CJ Bioscience Company; by the National Research Foundation of Korea (NRF) funded by the Korea government (MSIT) (RS-2025-00557272); and by a grant (RS-2025-02215737) from the Ministry of Food and Drug Safety (2025). The funder did not influence the results/outcomes of the study despite author affiliations with the funder.

Competing interests BEK, HP, HK, JI, JY, EY, GHS, SC, JEK, JMK, SYK, HSO, and AM are employed by CJ Bioscience. The remaining authors declare that they have no competing interests.

Patient consent for publication Not applicable.

Ethics approval The study was conducted in accordance with principles of Good Clinical Practice and approved by the institutional review boards from all centers (Yonsei Cancer Center, Samsung Medical Center, Caho Family Comprehensive Cancer Center, UPMC Hillman Cancer Center) IRB 4-2023-0715. Participants gave informed consent to participate in the study before taking part.

Provenance and peer review Not commissioned; externally peer reviewed.

Data availability statement All data relevant to the study are included in the article or uploaded as supplementary information.

ORCID iDs
Dong Kwon Kim https://orcid.org/0000-0002-1407-2369
Diwakar Davar https://orcid.org/0000-0002-7846-8055
Hyunkyung Park https://orcid.org/0009-0004-5855-2403
Junwon Yang https://orcid.org/0000-0002-9814-6918
Byoung Chul Cho https://orcid.org/0000-0002-5562-270X

REFERENCES

1 Lee JB, Kim HR, Ha SJ. Immune Checkpoint Inhibitors in 10 Years: Contribution of Basic Research and Clinical Application in Cancer Immunotherapy. *Immune Netw* 2022;22:e2.
2 Reck M, Rodríguez-Abreu D, Robinson AG, *et al*. Pembrolizumab versus Chemotherapy for PD-L1-Positive Non-Small-Cell Lung Cancer. *N Engl J Med* 2016;375:1823–33.
3 Gandhi L, Rodríguez-Abreu D, Gadgeel S, *et al*. Pembrolizumab plus Chemotherapy in Metastatic Non-Small-Cell Lung Cancer. *N Engl J Med* 2018;378:2078–92.
4 Bum Lee J, Huang Y, Oya Y, *et al*. Modulating the gut microbiome in non-small cell lung cancer: Challenges and opportunities. *Lung Cancer (Auckl)* 2024;194:107862.
5 Xie M, Li X, Lau HC-H, *et al*. The gut microbiota in cancer immunity and immunotherapy. *Cell Mol Immunol* 2025;22:1012–31.
6 Davar D, Dzutsev AK, McCulloch JA, *et al*. Fecal microbiota transplant overcomes resistance to anti-PD-1 therapy in melanoma patients. *Science* 2021;371:595–602.
7 Lee S-H, Cho S-Y, Yoon Y, *et al*. Bifidobacterium bifidum strains synergize with immune checkpoint inhibitors to reduce tumour burden in mice. *Nat Microbiol* 2021;6:277–88.
8 Min A, Synn C, Kang S, *et al*. Abstract 6433: A novel bacterial strain, CJRB-101, induces anti-cancer effects by repolarization of M2 to CXCL9 and CXCL10 dual expressing M1 macrophages in humanized non-small cell lung cancer mice models. *Cancer Res* 2023;83:6433.
9 Lee JB, Ahn JS, Nagasaka M, *et al*. First-in-human study of CJRB-101, a live biotherapeutic product in combination with pembrolizumab in selected types of advanced or metastatic cancer. *JCO* 2025;43:8547.
10 Chalita M, Kim YO, Park S, *et al*. EzBioCloud: a genome-driven database and platform for microbiome identification and discovery. *Int J Syst Evol Microbiol* 2024;74:006421.
11 Wood DE, Lu J, Langmead B. Improved metagenomic analysis with Kraken 2. *Genome Biol* 2019;20:257.
12 Chalita M, Ha SM, Kim YO, *et al*. Improved Metagenomic Taxonomic Profiling Using a Curated Core Gene-Based Bacterial Database Reveals Unrecognized Species in the Genus *Streptococcus Pathogens* 2020;9:204.
13 Langmead B, Salzberg SL. Fast gapped-read alignment with Bowtie 2. *Nat Methods* 2012;9:357–9.
14 Danecek P, Bonfield JK, Liddle J, *et al*. Twelve years of SAMtools and BCFtools. *Gigascience* 2021;10:giab008.
15 Quinlan AR, Hall IM. BEDTools: a flexible suite of utilities for comparing genomic features. *Bioinformatics* 2010;26:841–2.
16 Bolyen E, Rideout JR, Dillon MR, *et al*. Reproducible, interactive, scalable and extensible microbiome data science using QIIME 2. *Nat Biotechnol* 2019;37:852–7.
17 Martin M. Cutadapt removes adapter sequences from high-throughput sequencing reads. *EMBnet j* 2011;17:10.
18 Callahan BJ, McMurdie PJ, Rosen MJ, *et al*. DADA2: High-resolution sample inference from Illumina amplicon data. *Nat Methods* 2016;13:581–3.

19 Bokulich NA, Kaehler BD, Rideout JR, *et al*. Optimizing taxonomic classification of marker-gene amplicon sequences with QIIME 2's q2-feature-classifier plugin. *Microbiome* 2018;6:90.
20 Rognes T, Flouri T, Nichols B, *et al*. VSEARCH: a versatile open source tool for metagenomics. *PeerJ* 2016;4:e2584.
21 Kim DK, Synn C-B, Lee W, *et al*. Denfivontinib Activates Effector T Cells Through the NLRP3 Inflammasome, Yielding Potent Anticancer Effects by Combination with Pembrolizumab. *Mol Cancer Ther* 2025;24:354–69.
22 Jenkins RW, Aref AR, Lizotte PH, *et al*. *Ex Vivo* Profiling of PD-1 Blockade Using Organotypic Tumor Spheroids. *Cancer Discov* 2018;8:196–215.
23 Patnaik A, Kang SP, Rasco D, *et al*. Phase I Study of Pembrolizumab (MK-3475; Anti-PD-1 Monoclonal Antibody) in Patients with Advanced Solid Tumors. *Clin Cancer Res* 2015;21:4286–93.
24 Lindauer A, Valiathan CR, Mehta K, *et al*. Translational Pharmacokinetic/Pharmacodynamic Modeling of Tumor Growth Inhibition Supports Dose-Range Selection of the Anti-PD-1 Antibody Pembrolizumab. *CPT Pharmacometrics Syst Pharmacol* 2017;6:11–20.
25 Riely GJ, Wood DE, Aisner DL, *et al*. NCCN Guidelines® Insights: Non-Small Cell Lung Cancer, Version 7.2025. *J Natl Compr Canc Netw* 2025;23:354–62.